Advances in Engineering Software 173 (2022) 103204

Contents lists available at ScienceDirect

Advances in Engineering Software

journal homepage: www.elsevier.com/locate/advengsoft

Research paper

Smoothing topology optimization results using pre-built lookup tables

Zhi Li [a], Ting-Uei Lee [a], Yuan Yao [b], Yi Min Xie [a,*]

[a] Center for Innovative Structures and Materials, School of Engineering, RMIT University, Melbourne, 3001, Australia
[b] Ameba Engineering Structure Optimization Research Institute, Nanjing, 211800, China

ARTICLE INFO

Keywords:
Topology optimization
Smoothing
Finite element analysis
Volume-preserving
Area-preserving

ABSTRACT

Topology optimization techniques are typically performed on a design domain discretized with finite element meshes to generate efficient and innovative structural designs. The optimized structural topologies usually exhibit zig-zag boundaries formed from straight element edges. Existing techniques to obtain smooth structural topologies are limited. Most methods are computationally expensive, as they are performed iteratively with topology optimization. Other methods, such as post-processing methods, are applied after topology optimization, but they cannot guarantee to obtain equivalent structural designs, as the volume and geometric features may be changed. This study presents a new method that uses pre-built lookup tables to transform the shape of boundary elements obtained from topology optimization to create smoothed structural topologies. The new method is developed based on the combination of the bi-directional evolutionary structural optimization (BESO) technique and marching geometries to determine structural topologies and lookup tables, respectively. An additional step is used to ensure that the generated result meets a target volume. A variety of 2D and 3D examples are presented to demonstrate the effectiveness of the new method. This research shows that the new method is highly efficient, as it can be directly added to the last step of topology optimization with a low computational cost, and the volume and geometric features can be preserved in smoothed topologies. Finite element models are also created for original and smoothed structural topologies to show that the structural stiffness can be significantly enhanced after smoothing.

1. Introduction

Topology optimization is a structural optimization technique to obtain innovative structures that possess lightweight, high-performance and cost-efficient material characteristics [1]. As such, topology optimization techniques have been widely adopted across many disciplines, including additive manufacturing [2–4], architectural applications [5–7], furniture designs [8,9], and biological materials [10,11].

Topology optimization techniques typically use finite element analysis (FEA) to evaluate structural performance. To this end, many topology optimization techniques require the continuous design domain to be discretized into finite element meshes in order to conduct FEA, referring to element-based topology optimization approaches [12,13]. Popular element-based approaches include the solid isotropic material with penalization (SIMP) method [14,15] and the bi-directional evolutionary structural optimization (BESO) method [16,17]. The key difference between these two methods is the density representation of their elements. The SIMP method allows the densities of elements to vary continuously between 0 and 1 [18], while the BESO method only allows the densities of elements to be either 0 or 1 [16]. As a result, optimal structural topologies obtained from the SIMP method may possess "gray" boundaries corresponding to "soft" elements; BESO structural topologies may possess zig-zag boundaries formed from straight element edges [19]. It is worth pointing out that the resolution of these element-based topologies can be significantly increased using a large number of elements, which can create finer gray and zig-zag boundaries, and lead to visually smooth boundaries.

To generate smooth structural topologies, gray and zig-zag boundaries typically require further modifications [20]. Two dominant strategies in recent studies are *geometrically constrained topology optimization* methods and *post-processing* methods. The former strategy employs geometric operations during the optimization process, where smooth structural topologies are generated in each iteration [19,21–26]. However, such methods are computationally expensive due to the generation of unnecessary smoothed topologies throughout the optimization [20]. The latter strategy focuses on smoothing the generated optimal topologies, such as iso-surface extraction algorithms [27–30] and Laplacian smoothing techniques [31,32]. However, such methods cannot create smoothed models that are truly equivalent to the actual topology optimization results, as the volume or geometric features cannot be preserved in the generated models [20]. Baccialia

* Corresponding author.
E-mail address: mike.xie@rmit.edu.au (Y.M. Xie).

https://doi.org/10.1016/j.advengsoft.2022.103204
Received 14 February 2022; Received in revised form 23 May 2022; Accepted 23 July 2022
Available online 6 August 2022

et al. [33] have proposed a volume-preserved smoothing method that can obtain equivalent smooth models, but their method results in a performance loss of about 2%. Recently, Li et al. [34] have used a volume-preserved smoothing method to obtain smooth structural topologies. However, their method has not been extended to commonly used irregular elements such as tetrahedra.

For practical applications, computer-aided design (CAD) models are typically needed. However, the smoothed topologies fail to be directly converted into CAD models, especially in 3D cases [35]. They are recognized as non-manifold models in CAD software because their volumetric meshes include coincident faces and singularities [33,35]. The most straightforward strategy to overcome this problem is to rebuild a smoothed manifold CAD model [35]. In doing so, the generated model may differ from the actual topology optimization result regarding the volume and structural performance.

This paper presents a novel post-processing method (or smoothing method) to create smoothed manifold CAD models from element-based topology optimization results. The proposed method can transform the shape of elements using pre-built lookup tables straight after the topology optimization is completed, which can effectively and conveniently smooth the zig-zag boundaries. The new method is developed considering the equivalency of the original and smoothed structural topologies, meaning that the geometric features and volume can be preserved after smoothing. Section 2 first briefly summarizes the method of topology optimization and describes the details of the new smoothing method. Section 3 demonstrates the implementation of the new method and compares the differences between original and smoothed structural topologies. Section 4 discusses the effect of different mesh types and sizes in potential practical applications, followed by a conclusion in Section 5.

2. Methodology

2.1. BESO structural topology optimization

This study uses the soft-kill BESO method to perform structural topology optimization [16,36]. For a discretized design domain with N elements, the compliance minimization (or stiffness maximization) problem statement subject to a volume constraint can be written as follows.

$$Minimize: \quad C = \frac{1}{2}\mathbf{U}^T\mathbf{K}\mathbf{U} \tag{1a}$$

$$Subject\ to: \quad \mathbf{V}^* - \sum_{i=1}^{N}\mathbf{V}_i x_i = 0 \tag{1b}$$

$$x_i = x_{min} \text{ or } 1 \tag{1c}$$

where C is the compliance of the structure, $\mathbf{K}$ is the global stiffness matrix, $\mathbf{U}$ is the displacement vector, $\mathbf{V}^*$ is the target structural volume, and $\mathbf{V}_i$ is the volume of the ith element. The design variable, x_i, determines whether the ith element is solid ($x_i = 1$) or void ($x_i = x_{min} = 0.001$).

The material model of elements is defined as a function of the element density.

$$E(x_i)^k = {x_i}^p E_0 \tag{2}$$

where k is the current iteration number, $E(x_i)^k$ is the Young's modulus of ith element, E_0 is the design Young's modulus of elements, and $p = 3$ is the penalty exponent.

To relate the structural performance of elements to the optimization objective, ith elemental sensitivity number, $S_e(i)$, can be defined as

$$S_e(i) = -\frac{1}{p}\frac{\partial C}{\partial x_i} = \begin{cases} \frac{1}{2}\mathbf{u}_i^T\mathbf{K}_i^0\mathbf{u}_i & when\ x_i = 1 \\ \frac{x_{min}^{p-1}}{2}\mathbf{u}_i^T\mathbf{K}_i^0\mathbf{u}_i & when\ x_i = x_{min} \end{cases} \tag{3}$$

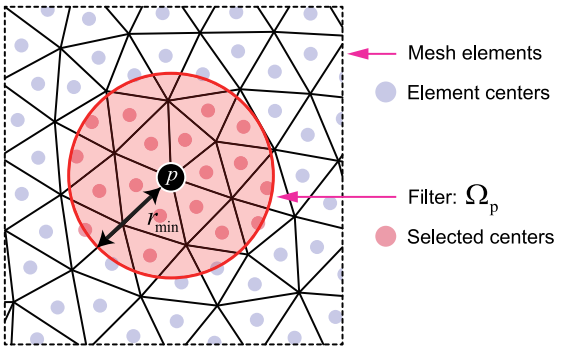

Fig. 1. Obtaining the nodal sensitivity field by employing a filter on mesh elements. This figure shows that the filter covers a circular domain Ω_p with a center of node p, which has a radius of r_{min}.

where $\mathbf{K}_i^0$ is the elemental stiffness matrix, and $\mathbf{u}_i$ is the displacement vector.

To improve the convergence of the BESO technique, historical sensitivity numbers can be averaged, where

$$\hat{S}_e(i) = \frac{S_e^k(i) + S_e^{k-1}(i)}{2} \tag{4}$$

The target volume for the next iteration, $\mathbf{V}^{k+1}$, depends on the current volume, $\mathbf{V}^k$, and a specified evolutionary ratio, ert, where

$$\mathbf{V}^{k+1} = \mathbf{V}^k(1 \pm ert) \tag{5}$$

Note that a threshold sensitivity number, S_{th}, is calculated based on $\mathbf{V}^{k+1}$ using the method described in [36]. Elements that possess the sensitivity number higher and lower than S_{th} are then preserved and removed, respectively. The optimization process is repeated until reaching the target volume and satisfying the convergence criteria [16].

2.2. Smoothing preparation

Once the element-based structural topology is obtained using the method described in Section 2.1, the nodal sensitivity field, S_n, is calculated for smoothing preparation. This can be achieved by employing a filter on elements [37,38], as shown in Fig. 1, where the filter covers a circular domain Ω_p with a center of node p. The filtering scheme is given as

$$S_n(p) = \frac{\sum_{q=1}^{N_n}(r_{min} - r_{pq})\hat{S}_e(q)}{\sum_{q=1}^{N_n}(r_{min} - r_{pq})} \tag{6}$$

where $S_n(p)$ is the sensitivity number of node p. N_n is the number of element centers covered by the filter. r_{min} is the filter radius, and r_{pq} is the distance between the center of element q and node p. It is noted that filtering all elements gives a nodal sensitivity field, S_n.

Finally, an iso-value, S_{iso}, is specified between the maximum and minimum S_n, that is, within the nodal sensitivity field, for further smoothing procedures as described below.

2.3. Smoothing 2D structural topologies

This sub-section describes a method to directly transform the shape of elements generated from topology optimization, so that smooth 2D structural topologies can be conveniently created. For a 2D structural topology, a level-set function can be created in its nodal sensitivity field [25,39]. Specifying S_{iso} determines the solid domain Ω_S, void domain Ω_V and boundary Γ, as shown in Fig. 2(c). For node p in the design domain, its (x, y, z) position, $\mathbf{p}$, related to S_{iso} can be described as

$$\begin{cases} \mathbf{p} \in \Omega_V, & if\ S_n(p) > S_{iso} \\ \mathbf{p} \in \Gamma, & if\ S_n(p) = S_{iso} \\ \mathbf{p} \in \Omega_S, & if\ S_n(p) < S_{iso} \end{cases} \tag{7}$$

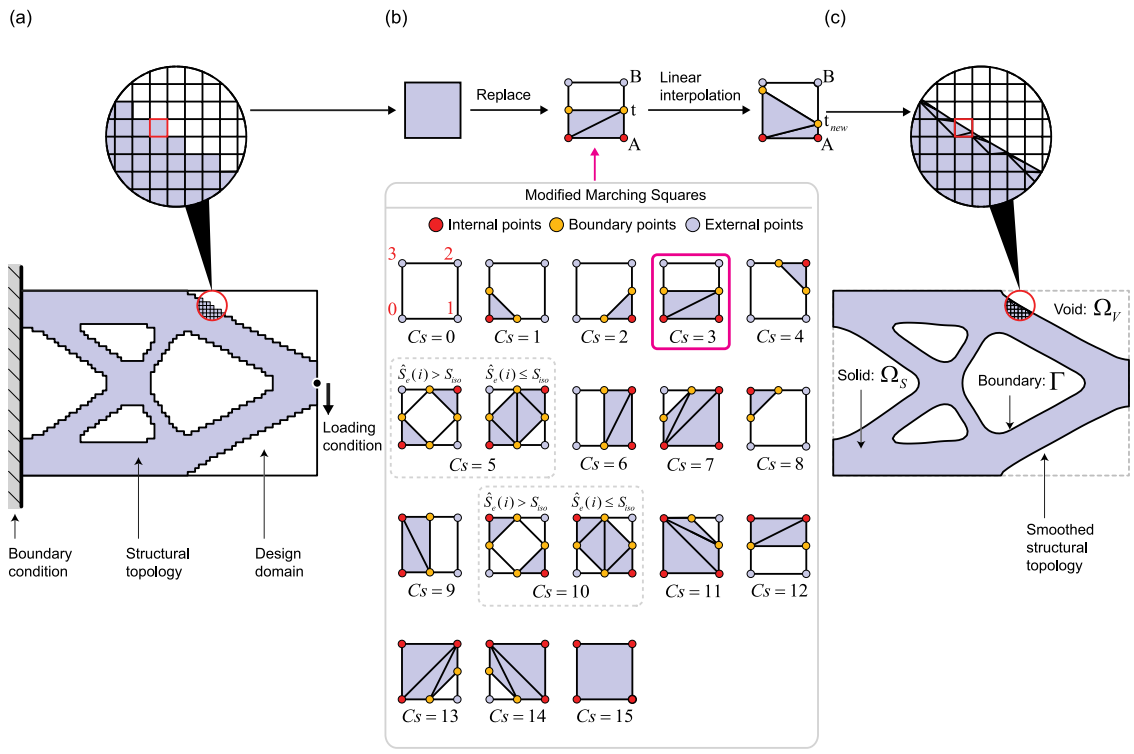

Fig. 2. Smoothing the structural topology of a 2D cantilever. (a) Initial setup of the optimization problem, where the design domain is discretized with quadrangular elements. (b) The lookup table is built using the modified Marching Squares algorithm that has 18 possible configurations. (c) The transformation result is obtained through reshaping all original elements.

$St(p)$ is introduced to determine whether $S_n(p)$ corresponds to solid, void, or boundary using 0 and 1 only, where

$$St(p) = \begin{cases} 0, & if\ S_n(p) > S_{iso} \\ 1, & if\ S_n(p) \le S_{iso} \end{cases} \tag{8}$$

This equation represents that void points are those with $St(p) = 0$, and both solid and boundary points possess $St(p) = 1$.

To transform the shape of structural elements, this study uses lookup tables to pre-define all possible transformation results of a unit element. For quadrangular elements shown in Fig. 2(a), the corresponding lookup table can be built by modifying the Marching Squares (MS) algorithm [40,41]. More specifically, the iso-lines in the original marching squares are replaced with pre-defined triangular or quadrangular meshes to represent solid domains, as shown in Fig. 2(b). Using Eq. (8), elemental nodes can be assigned with $St(p) = 1$ or 0 for internal (red) and external (gray) points, respectively. Additional boundary (orange) points are then created on the midpoint between internal and external points. Mathematically, there are 16 possible transformation results of a quadrangular element, calculated using

$$Cs(i) = \sum_{j=0}^{N_i} St(n_j)2^j \tag{9}$$

where Cs is the case number, N_i is the number of nodes of element i, and $St(n_j)$ represents the 0/1 state of jth node in element i; the number of possible cases is calculated as $2^{N_i} = 2^4 = 16$. However, there are actually 18 marching squares listed in the lookup table, as shown in Fig. 2(b).

It should be noted that the calculated Cs value may correspond to more than one marching geometry [42]. Such special cases occur when the diagonal corners are determined as internal (red) points, with the intermediate region surrounded by boundary (orange) points being either filled or vacant, resulting in connected and disconnected solid domains, respectively. In the present example, special cases are $Cs = 5$ and $Cs = 10$, with each containing two possible marching squares. Therefore, the total number of possible marching squares is 16+2 = 18. In this study, the selection of marching squares for special cases can be simply determined based on the averaged elemental sensitivity, $\hat{S}_e(i)$ (see Eq. (4)). Specifically, $\hat{S}_e(i) \le S_{iso}$ and $\hat{S}_e(i) > S_{iso}$ correspond to connected and disconnected solid domains, respectively.

Next, all elements in the design domain are reshaped using the modified MS lookup table. Finally, for each boundary (orange) point t between an internal (red) point A and an external (gray) point B, its (x, y, z) coordinate is relocated to a new position $\mathbf{t_{new}}$ using the following linear interpolation method, as shown in Fig. 2.

$$\mathbf{t_{new}} = \mathbf{A} + \frac{S_{iso} - S_n(A)}{S_n(B) - S_n(A)}(\mathbf{B} - \mathbf{A}) \tag{10}$$

where $\mathbf{A}$ and $\mathbf{B}$ are the (x, y, z) locations of the internal point A and external point B, respectively. $S_n(A)$ and $S_n(B)$ are filtered nodal sensitivity numbers of points A and B, respectively. It is noted that relocating all boundary points gives a smooth boundary.

Furthermore, the intersections between the generated structural topology and the design domain are unchanged after smoothing. This is because the elements located on the boundaries of the design domain possess $St = 1$ on their nodes.

To summarized, using Eq. (6) for all nodes creates a nodal sensitivity field, S_n, for a 2D structural topology. The specified iso-value, S_{iso}, determines the condition of each node, where $St = 0$ or 1, as described in Eqs. (8). In doing so, elements can be reshaped using the modified MS lookup table based on Eq. (9). Then, the shapes of the transformed elements are further updated using linear interpolation, as shown in Eq. (10). This 2D smoothing is demonstrated more clearly in Fig. 2.

2.4. Smoothing 3D structural topologies

3D structural topologies can also be smoothed based on different lookup tables, depending on the mesh element type. The two most common lookup tables are Marching Cubes (MC) [43] and Marching

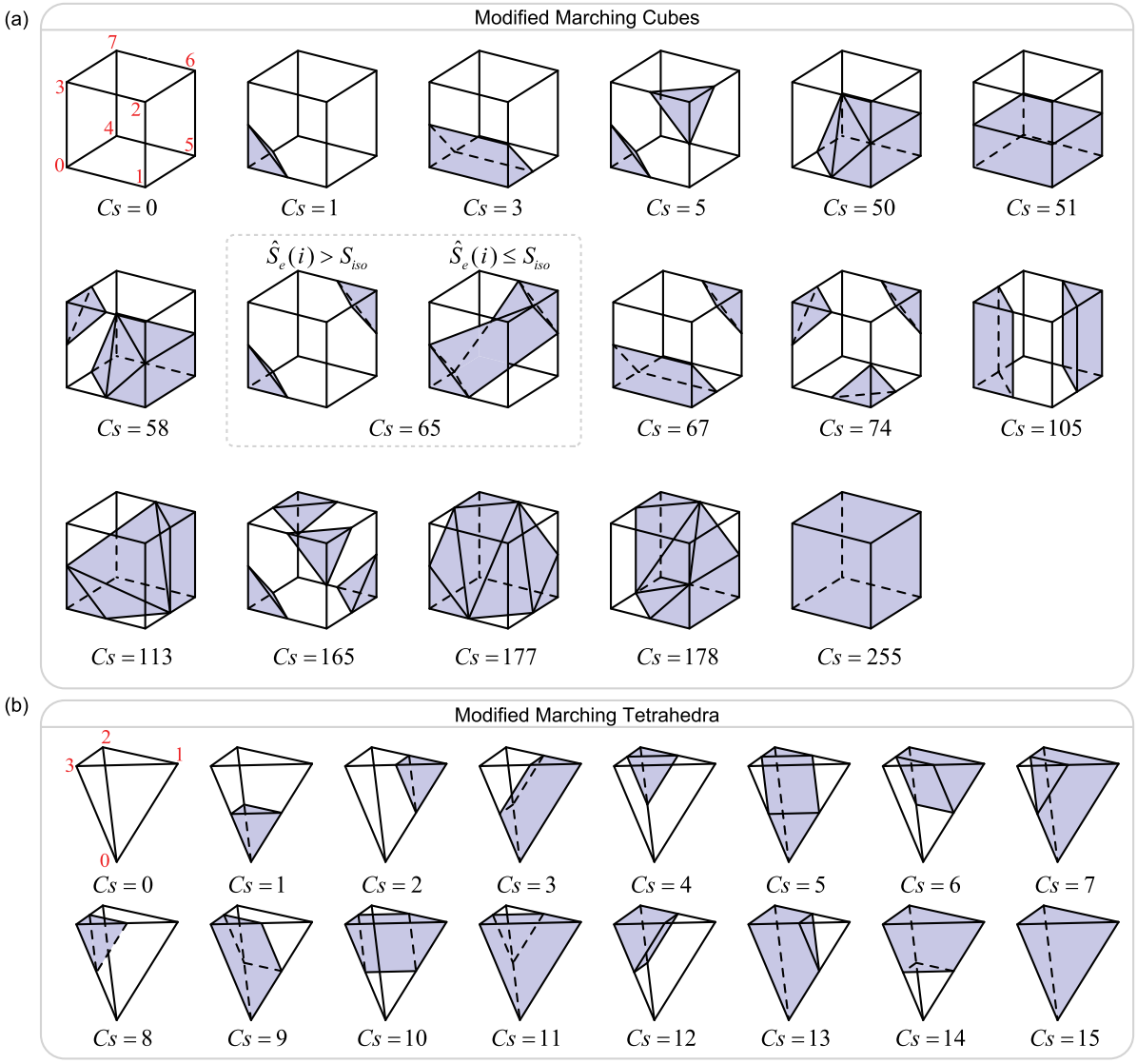

Fig. 3. Modified 3D lookup tables. The red numbers represent the indices of the elemental nodes. (a) 17 unique cases in the modified Marching Cubes method of a transformed hexahedral element. (b) All 16 possible cases in the modified MT method of a transformed tetrahedral element.

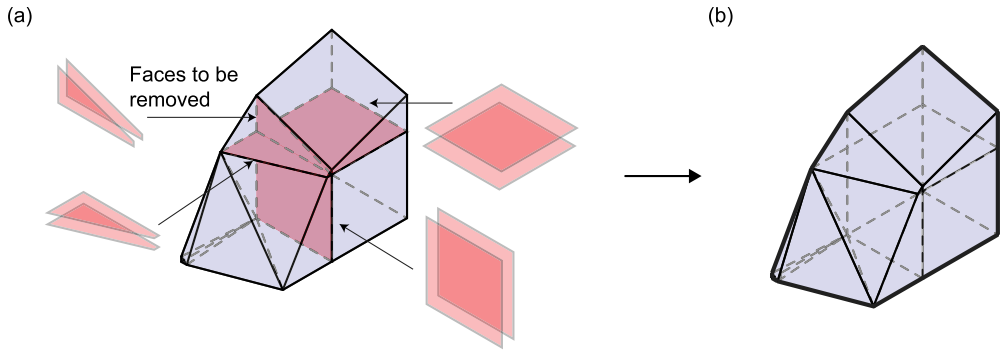

Fig. 4. Removing coincident faces of 3D elements. (a) All coincident faces are identified as internal faces, which are required to be removed. (b) Removing all internal faces gives a 3D closed surface mesh.

Tetrahedra (MT) [44] for hexahedral and tetrahedral mesh elements, respectively. Compared with the original MC and MT methods, the 3D transformation cases are pre-defined by closed surface meshes to represent solid domains, as shown in Figs. 3(a) and (b). It is worth pointing out that the 8-nodes hexahedral element can be transformed into 260 possible configurations, but Fig. 3(a) only shows 17 unique cases; the remaining $260 - 17 = 243$ cases can be obtained by rotating and mirroring these 17 cases. Among these 17 unique cases, $Cs = 65$ is the special case, where it contains two possible marching cubes, highlighted in Fig. 3(a). Similar to the previous 2D example, connected and disconnected solid domains for the present 3D case are selected when $\hat{S}_e(i) \le S_{iso}$ and $\hat{S}_e(i) > S_{iso}$, respectively.

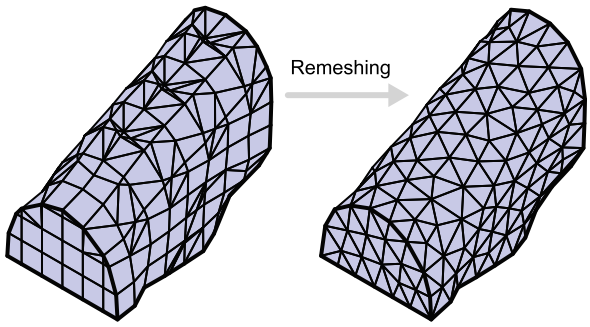

Fig. 5. Improve the surface quality using the incremental remeshing algorithm so that the elements on the surface can be re-distributed uniformly based on a target edge length and preserve the geometric features.

The entire smoothing process for 3D structural topologies is similar to the workflow developed for 2D cases. First, S_n is calculated for all nodes using Eq. (6). Second, S_{iso} is specified to assign all nodes with $St = 0$ or 1 based on S_n, as described in (8). Third, all elements are reshaped from the lookup table according to St using Eq. (9). Fourth, the shape of transformed elements are further modified using Eq. (10). Different to 2D smoothing, an additional step is required in 3D cases.

As shown in Fig. 4, this study removes all internal faces of 3D structural topologies. It should be highlighted that all transformed elements are closed surface meshes. They form a smoothed configuration that includes coincident faces, as shown in Fig. 4(a). These coincident faces are identified as internal faces. Removing all internal faces gives 3D surface meshes, as shown in Fig. 4(b), which can be considered as CAD-compatible manifold meshes.

2.5. Surface remeshing

The products of the above 2D and 3D smoothing processes are surface meshes [45]. As shown in Fig. 5, the quality of these surfaces can be improved through "surface remeshing". It should be noticed that many remeshing techniques are developed based on manifold CAD models like surface meshes [46].

This study uses the incremental remeshing algorithm described in [45,47,48]. This algorithm can be found in many CAD software, such as Rhino 7. The remeshing algorithm repeatedly modifies the mesh edges and vertices based on local operations until all edge lengths are close to the prescribed target value; the local operations include splitting long edges, collapsing short edges, flipping mesh edges, and relocating vertices. As a result (see Fig. 5), the elements on the surface can be re-distributed uniformly using triangular elements toward the target edge length. It can also be seen that the geometric features, such as corners and sharp edges, are preserved during the remeshing process.

2.6. Preserving area or volume

The smoothed configurations obtained from the above methods can be understood as iso-sensitivity models, as they are determined based on the S_{iso} value. Moreover, changing S_{iso} can directly influence the final area and volume of 2D and 3D iso-sensitivity models, respectively. In order to meet a target area or volume, this study treats S_{iso} as a variable and introduces the bisection method to modify S_{iso} automatically.

$$S_{iso} = \frac{S_{up} + S_{lo}}{2} \tag{11}$$

where $S_{lo} = 0$ and $S_{up} = 2 \times S_{th}$ are the initial lower and upper bound, respectively. The S_{th} is the threshold sensitivity number mentioned in Section 2.1. The bounds are updated using

$$\begin{cases} S_{lo} = S_{iso}, & if\ V > V^* \\ S_{up} = S_{iso}, & if\ V \le V^* \end{cases} \tag{12}$$

where V is the current volume/area of the iso-sensitivity model, and V^* is the target volume/area.

The bi-sectional iterative process is repeated until

$$\frac{|V - V^*|}{V_D} \le V_{tol} \tag{13}$$

where V_D is the total volume/area of the design domain, $V_{tol} = 0.1\%$ is the allowable tolerance. This equation simply represents that the final structural topology will possess the total volume/area close to the target value with an acceptable difference. The entire smoothing process that considers preserving area or volume process is summarized in the flowchart shown in Fig. 6.

3. Numerical analysis

A numerical analysis method is developed to examine the capabilities of the above smoothing methods. More specifically, the obtained BESO structural topologies are compared with their corresponding smoothed results to observe any variations in shape and structural performance.

This study uses the commercial finite element analysis (FEA) software, Abaqus, and a Python script to perform structural analysis and BESO topology optimization, respectively, with details fully described in [36]. Once the optimal structural topologies are obtained, a C# code is used to execute the above algorithms for generating smoothed models in the Rhino 7 CAD software. The original and smoothed optimal structural topologies are then imported into Abaqus to perform FE structural analysis to compare their stiffness performance. In order to have a fair comparison, their FE meshes are set to have the same mesh type and target edge length. Specifically, 2D and 3D cases are analyzed using triangular and tetrahedral elements, respectively, with the target edge length set to be the same value as used in the remeshing process. Note that equivalent topologies are discretized using the same meshing algorithm embedded in the commercial Abaqus software to create FE models; meshing algorithms of FE models are not included in the scope of this study.

The material used in this study is assumed to be isotropic and linear elastic, with Young's modulus of $E = 1$ MPa and Poisson's ratio of $\upsilon = 0.3$. Unless otherwise stated, BESO topology optimization parameters are: $ert = 2\%$, $p = 3$, and $r_{min} = 3$ mm.

The 3D smoothing process is first tested using a cantilever example, as shown in Fig. 7. With reference to Fig. 7(a), the design domain of the cantilever is 60 mm × 10 mm × 40 mm. A $F = -1\ N$ point load is applied at the center of the free end. A fixed boundary condition is assigned behind the whole cantilever. The objective volume faction of BESO is set as 15%. Smoothed configurations are obtained from structural topologies with different mesh sizes, as shown in Figs. 7(a)–(b) and (c)–(d). For original BESO structural topologies, solid cubic elements that have an edge length of 1 mm and 0.5 mm are used, as shown in Figs. 7(a) and (c), respectively. For smoothed structural topologies, original elements are reshaped using the modified MC lookup table and then the assemblies are remeshed to a surface mesh with triangular elements that have an average edge length of 0.5 mm, as shown in Figs. 7(b) and (d). All structural topologies are discretized using solid tetrahedral elements with an edge length of 0.5 mm in FEA, so that the compliance values, C, are comparable.

In Fig. 7, it can be seen that the zig-zag boundaries of original structural topologies have been successfully smoothed. It can also be seen that the geometrical features have been preserved, where the shapes of the original and smoothed structural topologies are almost identical. Moreover, the structural volumes are changed within an allowable tolerance. Together, it can be concluded that the proposed smoothing method can generate equivalent structural topologies to the original topology optimization results.

Furthermore, the compliance of Figs. 7(a)–(d) are 5.336 Nmm, 4.855 Nmm, 5.060 Nmm, and 4.973 Nmm, respectively. It is seen that

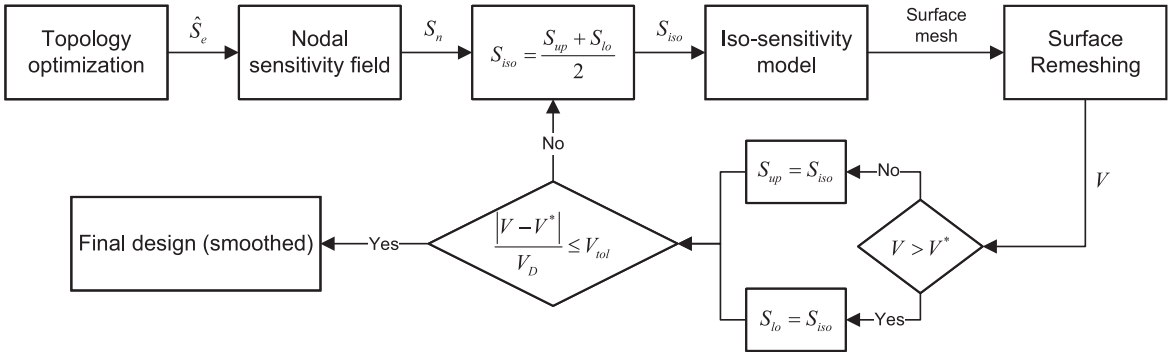

Fig. 6. The flowchart of the entire smoothing process. The process of preserving area or volume will ensure that the smoothed result meets a target area or volume.

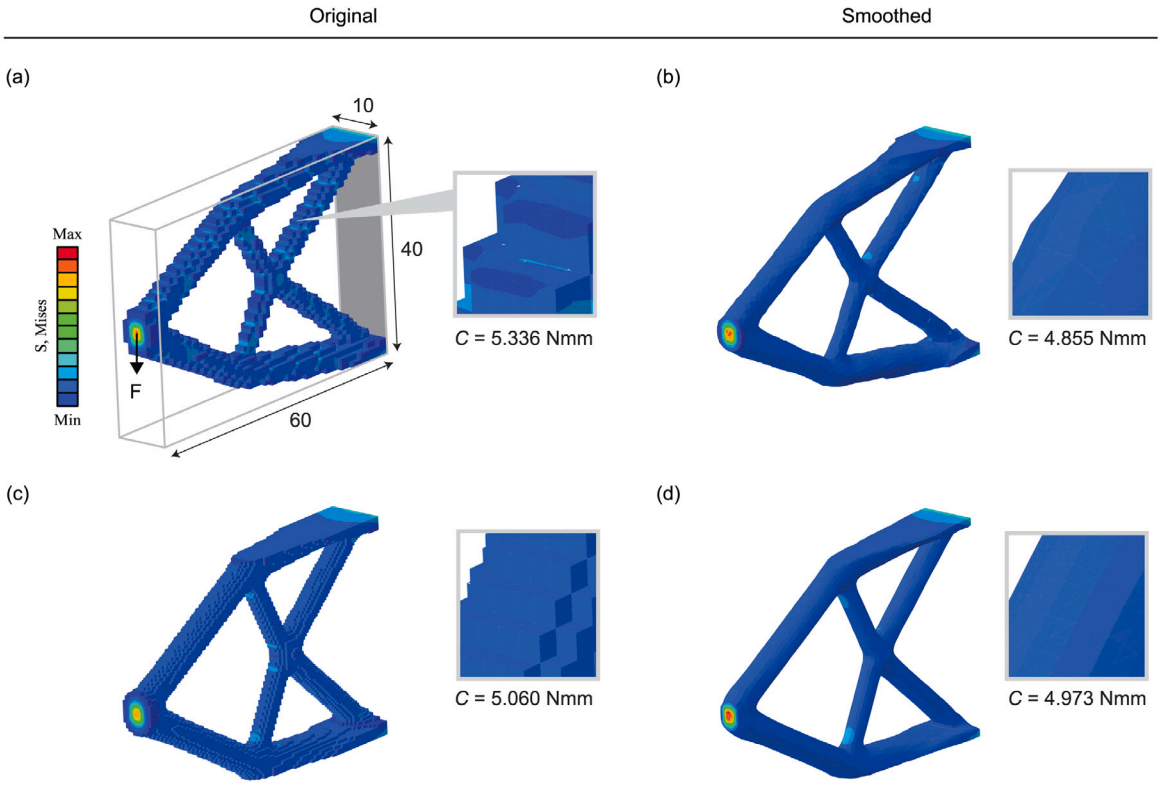

Fig. 7. FE results of original and smoothed structural topologies. (a)–(b) shows that cubic elements that have an edge length of 1 mm are smoothed into a surface mesh with triangular elements that have an average edge length of 0.5 mm. (c)–(d) shows that cubic elements that have an edge length of 0.5 mm are smoothed into a surface mesh with triangular elements that have an average edge length of 0.5 mm. (a) and (c) are original structural topologies; (b) and (d) are smoothed structural topologies. In FEA (a)–(d) are meshed using solid tetrahedral elements with an average edge length of 0.5 mm.

the smoothed structures are stiffer, corresponding to lower compliance. More specifically, the compliance of Figs. 7(a) and (c) are reduced by 9.02% and 1.73% after smoothing, respectively. The enhanced structural performance may be attributed to the stress being more uniformly distributed in the smoothed models, thus resulting in lower compliance, demonstrated more clearly in Figs. 7(a)–(b). However, the improvement is less noticeable using a finer mesh, as the resolution of the original structural topology is already high, meaning that the shape is similar to its corresponding smoothed form, as shown in Figs. 7(c)–(d). Nevertheless, this example still demonstrates that an enhanced structural performance can be obtained through smoothing.

4. Discussion

4.1. Regular and irregular 2D meshes

This subsection examines the structural performance of smoothed topologies obtained from regular and irregular 2D quadrangular meshes [49], as shown in Figs. 8(a) and (b), respectively.

Fig. 8(a) shows a 240 mm × 40 mm MBB beam initially meshed with 1 mm square elements. A $F = -1\ N$ point load is applied at the midpoint of the top edge. For topology optimization, the objective volume faction is set as 50%, and r_{min} is changed to 2 mm. During the smoothing process, the modified MS lookup table is used to obtain

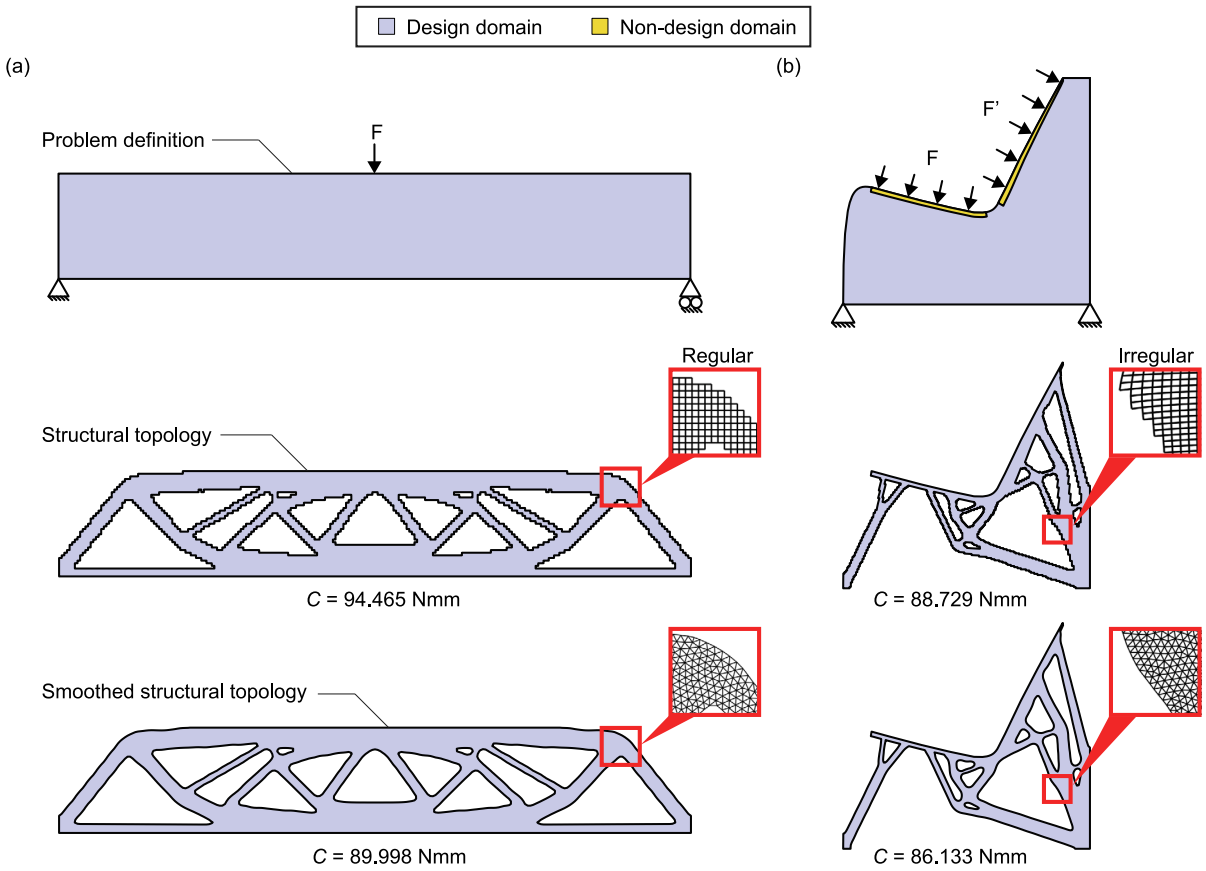

Fig. 8. Smoothing 2D structural topologies with regular and irregular meshes. Sub-figures from the top are: optimization problem, original structural topology, and smoothed structural topology. (a) MBB beam example initially meshed with square elements. (b) Chair example initially meshed with irregular quadrangular elements.

transformed quadrangular elements, and then they are remeshed using triangular elements with an average edge length of 1 mm. For FE structural analysis, the original and smoothed structural topologies are both discretized using triangular elements with an average edge length of 1 mm.

In Fig. 8(a), it can be seen that the MBB beam has been successfully smoothed using the proposed 2D smoothing method, which reduces the original compliance by 3.46% (from 94.465 Nmm to 89.998 Nmm). The same example has been smoothed previously using the FTOP method [23] with a final compliance of 89.68 Nmm, which is similar to the present smoothed result in shape and compliance. However, the FTOP method requires more than 300 iterations to obtain the final smoothed result with smoothed structural topologies generated in each iteration. In contrast, the proposed smoothing method is much more efficient, which can be added to the last step of the BESO process. This example only uses 70 iterations to obtain the structural topology, and the total time spent on the smoothing process is only 0.43 s using an ordinary laptop with an Intel i7-9750H 2.60 GHz processor.

The 777 mm × 713 mm chair example shown in Fig. 8(b) is initially meshed with irregular quadrangular elements in order to create smooth boundaries, resulting in all elements having different shapes with an averaged edge length of 4.25 mm. The chair is loaded at its non-design domains with a relative force density of $F : F' = 3 : 2$ [50], where $F = 0.03\ N$ and $F' = 0.02$ N. The objective volume faction is set as 33% to obtain the BESO structural topology. In terms of smoothing process, the modified MS lookup table in Fig. 2(b) is used, where each sub-figure may be reshaped depending on the shape of the selected irregular element using Eq. (10). Finally, the transformed elements are remeshed using triangular elements that have an average edge length of 3.5 mm. For FE structural analysis, the original and smoothed structural topologies are both discretized using triangular elements with an average edge length of 3.5 mm.

In Fig. 8(b), it is seen that the chair has been successfully smoothed, meaning that the proposed smoothing method is capable of dealing with irregular meshes. Similar to the above examples with regular meshes, the compliance also reduces after smoothing, where a 2.93% improvement is achieved; C is reduced from 88.729 Nmm to 86.133 Nmm. It is worth pointing out that complex geometries are typically discretized with irregular meshes to perform topology optimization. Using the proposed method, optimal structural topologies of such complex geometries can be conveniently smoothed, which means that the proposed method is highly beneficial for complex geometries initially discretized with irregular meshes.

4.2. 3D Practical application

A 771 mm × 400 mm × 713 mm 3D chair example is given here to demonstrate the potential practical applications of the proposed smoothing method, as shown in Fig. 9. Fig. 9(a) shows the setup of the optimization problem, from which 81% of the material is removed through topology optimization. It is assumed that the chair carries an 80 kg adult, hence the non-design domain is loaded with $F = 0.0003$ N/mm^2 and $F' = 0.0002$ N/mm^2 on the seat part and the back-rest part, respectively [50]. Four 20 mm × 20 mm regions on the bottom surface are assigned to have a fixed boundary condition. r_{min} is changed to 30 mm to obtain the BESO structural topology. The modified MT lookup table is used for smoothing. The original and smoothed chairs are both meshed with solid tetrahedra that have an edge length of 10 mm.

Figs. 9(b)–(c) show the original and smoothed structural topologies, respectively. It is seen that the smoothed result improves not only the visual effect but also the structural performance, where the compliance of the original result is reduced by 6.52% (from 61.231 Nmm to 57.235

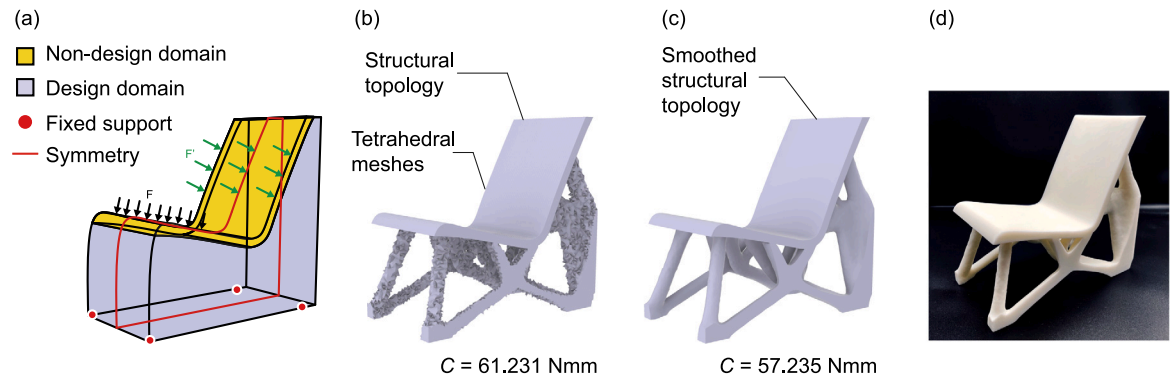

Fig. 9. Potential practical applications of the proposed smoothing method demonstrated with a 3D chair example. (a) Initial setup of the optimization problem. (b) Original structural topology obtained from topology optimization. (c) Smoothed structural topology. (d) Manufactured 3D model.

Nmm). Following the discussion of Section 4.1, complex 3D geometries are typically discretized with irregular tetrahedral meshes. After performing topology optimization on such complex 3D geometries, the proposed smoothing method can then be employed to create manifold CAD models that possess smooth boundaries, as shown in Figs. 9(c)–(d). Therefore, it is confirmed that the proposed smoothing method can be effectively adopted for 3D applications without the limitation of the mesh element type.

5. Conclusion

In this work, a new post-processing method is proposed, which uses pre-built lookup tables to smooth the zig-zag boundaries obtained from topology optimization. It is shown that the modified Marching Squares (MS), Marching Cubes (MC), and Marching Tetrahedra (MT) provide effective lookup tables for structures initially discretized with quadrangular (2D), hexahedral (3D), and tetrahedral (3D) elements, respectively. A series of examples are tested to show that: (1) the new method can create smooth structural topologies that preserve the volume and geometric features from the original optimal topologies, and (2) the compliance can be reduced after smoothing to achieve stiffer structures. Moreover, the new method is shown to be highly efficient, as it is performed as a post-processing step after the topology optimization is completed. This study also shows that the proposed method supports various mesh element types. Finally, a complex 3D example is used to demonstrate that the new method can be readily applied to a wide range of practical applications.

CRediT authorship contribution statement

Zhi Li: Conceptualization, Methodology, Software, Data curation, Validation, Visualization, Writing – original draft. **Ting-Uei Lee:** Writing – original draft, Visualization, Writing – review & editing. **Yuan Yao:** Conceptualization, Methodology. **Yi Min Xie:** Conceptualization, Methodology, Supervision, Writing – review & editing, Funding acquisition.

Declaration of competing interest

The authors declare that they have no known competing financial interests or personal relationships that could have appeared to influence the work reported in this paper.

Acknowledgments

This work was supported by the Australian Research Council [grant number FL190100014]. The authors would like to thank Yulin Xiong, Yunzhen He, James Kirby, Qiang Zhou, Qin Yang, Jiaming Ma and Minghao Bi for their helpful advice on various technical issues examined in this paper.

References

[1] Bendsøe MP, Sigmund O. Topology optimization: theory, methods, and applications. 2th ed.. Springer; 2004.
[2] Xiong YL, Yao S, Zhao ZL, Xie YM. A new approach to eliminating enclosed voids in topology optimization for additive manufacturing. Addit Manuf 2020;32:101006. http://dx.doi.org/10.1016/j.addma.2019.101006.
[3] Bi M, Tran P, Xie YM. Topology optimization of 3D continuum structures under geometric self-supporting constraint. Addit Manuf 2020;36:101422. http://dx.doi.org/10.1016/j.addma.2020.101422.
[4] Xu B, Han Y, Zhao L, Xie YM. Topological optimization of continuum structures for additive manufacturing considering thin feature and support structure constraints. Eng Optim 2020;53(12):2122–43. http://dx.doi.org/10.1080/0305215X.2020.1849170.
[5] Aage N, Amir O, Clausen A, Hadar L, Maier D, Søndergaard A. Advanced topology optimization methods for conceptual architectural design. In: Proceedings of the advances in architectural geometry 2014. Cham: Springer; 2015, p. 159–79.
[6] Xie YM, Zuo ZH, Huang X, Tang JW, Zhao B, Felicetti P. Architecture and urban design through evolutionary structural optimisation algorithms. In: Proceedings of the international symposium on algorithmic design for architecture and urban design, Tokyo. 2011.
[7] Cui C, Ohmori H, Sasaki M. Computational morphogenesis of 3d structures by extended ESO method. J Int Assoc Shell Spatial Struct 2003;44(1):51–61. http://dx.doi.org/10.1016/j.engstruct.2014.07.032.
[8] Bhooshan V, Fuchs M, Bhooshan S. 3D-printing, topology optimization and statistical learning: a case study. In: Symposium on simulation for architecture and urban design, Toronto. 2017, p. 1–8.
[9] Ma J, Li Z, Zhao ZL, Xie YM. Creating novel furniture through topology optimization and advanced manufacturing. Rapid Prototyp J 2021;27(9):1749–58. http://dx.doi.org/10.1108/RPJ-03-2021-0047.
[10] Zhao ZL, Zhou SW, Feng XQ, Xie YM. On the internal architecture of emergent plants. J Mech Phys Solids 2018;119:224–39. http://dx.doi.org/10.1016/j.jmps.2018.06.014.
[11] Ma J, Zhao ZL, Lin S, Xie YM. Topology of leaf veins: experimental observation and computational morphogenesis. J Mech Beha Biomed 2021;123:104788. http://dx.doi.org/10.1016/j.jmbbm.2021.104788.
[12] Bendsøe MP, Kikuchi N. Generating optimal topologies in structural design using a homogenization method. Comput Meth Appl Mech Engrg 1998;71(2):197–224. http://dx.doi.org/10.1016/0045-7825(88)90086-2.
[13] Huang X, Xie YM. A new look at ESO and BESO optimization methods. Struct Multidiscip Optim 2008;35:89–92. http://dx.doi.org/10.1007/s00158-007-0140-4.
[14] Sigmund O. A 99 line topology optimization code written in matlab. Struct Multidiscip Optim 2001;21:120–7. http://dx.doi.org/10.1007/s001580050176.
[15] Sigmund O, Maute K. Topology optimization approaches. Struct Multidiscip Optim 2013;48:1031–55. http://dx.doi.org/10.1007/s00158-013-0978-6.
[16] Huang X, Xie YM. Evolutionary topology optimization of continuum structures: methods and applications. John Wiley & Sons; 2010.
[17] Huang X, Xie YM. Bi-directional evolutionary topology optimization of continuum structures with one or multiple materials. Comput Mech 2009;43:393–401. http://dx.doi.org/10.1007/s00466-008-0312-0.
[18] Bendsøe MP, Sigmund O. Material interpolation schemes in topology optimization. Arch Appl Mech 1999;69:635–54. http://dx.doi.org/10.1007/s004190050248.
[19] Fu YF, Rolfe B, Wang Y, Huang X, Ghabraie K. SEMDOT: smooth-edged material distribution for optimizing topology algorithm. Adv Eng Softw 2020;150:102921. http://dx.doi.org/10.1016/j.advengsoft.2020.102921.
[20] Subedi SC, Verma CS, Suresh K. A review of methods for the geometric post-processing of topology optimized models. J Comput Inf Sci Eng 2020;20(6):060801. http://dx.doi.org/10.1115/1.4047429.

[21] Zhuang Z, Xie YM, Zhou SW. A reaction diffusion-based level set method using body-fitted mesh for structural topology optimization. Comput Meth Appl Mech Eng 2021;381:113829. http://dx.doi.org/10.1016/j.cma.2021.113829.
[22] Fu YF, Rolfe B, Chiu LNS, Wang Y, Huang X, Ghabraie K. Smooth topological design of 3D continuum structures using elemental volume fractions. Comput Struct 2020;231:106213. http://dx.doi.org/10.1016/j.compstruc.2020.106213.
[23] Huang X. Smooth topological design of structures using the floating projection. Eng Struct 2020;208:110330. http://dx.doi.org/10.1016/j.engstruct.2020.110330.
[24] Huang X. On smooth or 0/1 designs of the fixed-mesh element-based topology optimization. Adv Eng Softw 2021;151:102942. http://dx.doi.org/10.1016/j.advengsoft.2020.102942.
[25] Da D, Xia L, Li G, Huang X. Evolutionary topology optimization of continuum structures with smooth boundary representation. Struct Multidiscip Optim 2018;57:2143–59. http://dx.doi.org/10.1007/s00158-017-1846-6.
[26] Martínez-Frutos J, Herrero-Pérez D. Gpu acceleration for evolutionary topology optimization of continuum structures using isosurfaces. Comput Struct 2017;182:119–36. http://dx.doi.org/10.1016/j.compstruc.2016.10.018.
[27] Koguchi A, Kikuchi N. A surface reconstruction algorithm for topology optimization. Eng Comput 2006;22:1–10. http://dx.doi.org/10.1007/s00366-006-0023-0.
[28] Marsan AL, Dutta D. Construction of a surface model and layered manufacturing data from 3D homogenization output. J Mech Des 1996;118(3):412–8. http://dx.doi.org/10.1115/1.2826901.
[29] Yoely YM, Amir O, Hanniel I. Topology and shape optimization with explicit geometric constraints using a spline-based representation and a fixed grid. Procedia Manuf 2018;21:189–96. http://dx.doi.org/10.1016/j.promfg.2018.02.110.
[30] Jiang C, Wang H, Inza VC, Dellinger F, Rist F, Wallner J, et al. Using isometries for computational design and fabrication. ACM Trans Graph 2021;40(4):1–12. http://dx.doi.org/10.1145/3450626.3459839.
[31] Ji Z, Liu L, Wang G. A global laplacian smoothing approach with feature preservation. In: Ninth international conference on computer aided design and computer graphics. Hong Kong: IEEE; 2005, p. 269–74.
[32] Field DA. Laplacian smoothing and delaunay triangulations. Commun Appl Numer Meth 1998;4(6):709–12. http://dx.doi.org/10.1002/cnm.1630040603.
[33] Bacciaglia A, Ceruti A, Liverani A. Surface smoothing for topological optimized 3D models. Struct Multidiscip Optim 2021;64:3453–72. http://dx.doi.org/10.1007/s00158-021-03027-6.
[34] Li X, Qin C, Wei P, Su C. A boundary density evolutionary topology optimization of continuum structures with smooth boundaries. Int J Numer Meth Eng 2022;123(1):158–79. http://dx.doi.org/10.1002/nme.6851.
[35] Larsen S, Jensen CG. Converting topology optimization results into parametric CAD models. Comput Aided Des Appl 2009;6(3):407–18. http://dx.doi.org/10.3722/cadaps.2009.407-418.
[36] Zuo ZH, Xie YM. A simple and compact python code for complex 3D topology optimization. Adv Eng Softw 2015;85:1–11. http://dx.doi.org/10.1016/j.advengsoft.2015.02.006.
[37] Sigmund O, Petersson J. Numerical instabilities in topology optimization: a survey on procedures dealing with checkerboards, mesh-dependencies and local minima. Struct Optim 1998;16:68–75. http://dx.doi.org/10.1007/BF01214002.
[38] Bourdin B. Filters in topology optimization. Int J Numer Meth Eng 2001;50(9):2143–58. http://dx.doi.org/10.1002/nme.116.
[39] Dervieux A, Thomasset F. A finite element method for the simulation of a Rayleigh–Taylor instability. In: Approximation methods for Navier–Stokes problems. Berlin: Springer; 1980, p. 145–58.
[40] Maple C. Geometric design and space planning using the marching squares and marching cube algorithms. In: Proceedings of the IEEE international conference on geometric modeling and graphics. London: IEEE; 2003, p. 90–5.
[41] Gong S, Newman TS. A corner feature sensitive marching squares. In: 2013 Proceedings of IEEE southeastcon. Jacksonville: IEEE; 2013, p. 1–6.
[42] Lachaud JO. Topologically defined iso-surfaces. In: Miguet S, Montanvert A, Ubéda S, editors. Discrete geometry for computer imagery. Berlin: Springer; 1996, p. 13–5.
[43] Lorensen WE, Cline HE. Marching cubes: a high resolution 3D surface construction algorithm. ACM SIGGRAPH Comput Graph 1987;21(4):163–9. http://dx.doi.org/10.1145/37401.37422.
[44] Doi A, Koide A. An efficient method of triangulating equi-valued surfaces by using tetrahedral cells. IEICE Trans Inf Syst 1991;74(1):214–24.
[45] Botsch M, Kobbelt L, Pauly M, Alliez P, Lévy B. Polygon mesh processing. CRC press; 2010.
[46] Surazhsky V, Gotsman C. Explicit surface remeshing. In: Proceedings of the 2003 Eurographics/ACM SIGGRAPH symposium on geometry processing. 2003, p. 20–30.
[47] Kobbelt L, Botsch M. A remeshing approach to multiresolution modeling. In: Proceedings of the 2004 Eurographics/ACM SIGGRAPH symposium on geometry processing. 2004, p. 185–92.
[48] Kobbelt L, Bareuther T, Seidel HP. Multiresolution shape deformations for meshes with dynamic vertex connectivity. Comput Graph Forum 2000;19(3):249–60. http://dx.doi.org/10.1111/1467-8659.00417.
[49] Chloe A. Meshing in FEA: structured vs unstructured meshes. 2020, https://onscale.com/blog/meshing-in-fea-structured-vs-unstructured-meshes/. [Accessed 13 October 2021].
[50] Zhu H. Modeling of pressure distribution of human body load on an office chair seat. (Master Thesis), Karlskrona, Sweden: Department of Mechanical Engineering, Blekinge Institute of Technology 2013.